Transcranial current stimulation focality using disc and ring electrode configurations: FEM analysis

Abhishek Datta[1]**, Maged Elwassif**[1]**, Fortunato Battaglia**[2] **and Marom Bikson**[1,3]

[1] Department of Biomedical Engineering, The City College of New York of the City University of New York, NY 10031, USA
[2] Sophie Davis School of Biomedical Education, The City College of New York of the City University of New York, NY 10031, USA

E-mail: bikson@ccny.cuny.edu

Abstract
We calculated the electric fields induced in the brain during transcranial current stimulation (TCS) using a finite-element concentric spheres human head model. A range of disc electrode configurations were simulated: (1) distant-bipolar; (2) adjacent-bipolar; (3) tripolar; and three ring designs, (4) belt, (5) concentric ring, and (6) double concentric ring. We compared the focality of each configuration targeting cortical structures oriented normal to the surface ('surface-radial' and 'cross-section radial'), cortical structures oriented along the brain surface ('surface-tangential' and 'cross-section tangential') and non-oriented cortical surface structures ('surface-magnitude' and 'cross-section magnitude'). For surface-radial fields, we further considered the 'polarity' of modulation (e.g. superficial cortical neuron soma hyper/depolarizing). The distant-bipolar configuration, which is comparable with commonly used TCS protocols, resulted in diffuse (un-focal) modulation with bi-directional radial modulation under each electrode and tangential modulation between electrodes. Increasing the proximity of the two electrodes (adjacent-bipolar electrode configuration) increased focality, at the cost of more surface current. At similar electrode distances, the tripolar-electrodes configuration produced comparable peak focality, but reduced radial bi-directionality. The concentric-ring configuration resulted in the highest spatial focality and uni-directional radial modulation, at the expense of increased total surface current. Changing ring dimensions, or use of two concentric rings, allow titration of this balance. The concentric-ring design may thus provide an optimized configuration for targeted modulation of superficial cortical neurons.

(Some figures in this article are in colour only in the electronic version)

Introduction

Transcranial current stimulation (TCS) involves the application of currents through electrodes on the scalp to modulate brain activity. Transcranial electrical stimulation (TES) conventionally refers to short-duration (50–500 μs)

[3] Current Address: T-403B, Steinman Hall, Department of Biomedical Engineering, The City College of New York, 140th street and Convent Avenue, New York, NY 10031, USA.

supra-threshold pulses (100–1200 V) [1–3]. Cranial electrotherapy stimulation (CES) utilizes a range of waveforms with peak current levels ranging from 50 μA to 5 mA [4]. Supra-threshold current pulse trains ($\sim$0.9 A) are generally used during electroconvulsive therapy (ECT) [5]. DC waveforms normally ranging from 260 μA to 2 mA are used for transcranial direct current stimulation (tDCS) [6–10]. The objective of this study was to examine optimized electrode configurations and to develop 'modulation maps'

that may guide anatomically and functionally targeted TCS applications.

Generally, TCS electrode configurations utilize one anode and one cathode, positioned around the head. tDCS applied to M1 can facilitate implicit learning [11] and tDCS over the occipital cortex can facilitate visuo-motor learning [12]. tDCS has also been shown to alter excitability or related behavioural performance in somatosensory [13], frontopolar [14] and prefrontal cortices [15]. Clinical TCS is being actively explored as a non-invasive therapeutic option for the treatment of neurological and psychiatric disorders including depression, stroke, epilepsy, learning disorders and for relieving pain [16–21].

Experimental and theoretical studies examining the mechanisms of TCS have implicated 'direct' modulation (polarization) of primary cortical neurons [8, 22, 23] and/or modulation of (NMDA) synaptic efficacy [24, 25]. Anode- and cathode-specific modulation of brain activity has been characterized using broad indicators of 'excitability' [8, 22, 26–30]. Oscillating transcranial currents can entrain cortical oscillations [4, 31]. *In vivo* [32] and *in vitro* [33–35] animal studies have identified complex short- and long-term actions on neuronal excitability. Despite clinical success with existing TCS technology, efficacy and targeting concerns include (1) divergent cathodal and anodal effects [30, 36]; (2) poor spatial focality [37, 38] and (3) poorly characterized cellular targets (e.g. neuronal type) and biophysics of both short- and long-term modulation [33, 34, 39–41]. Clinical protocols are thus adjusted empirically and restricted within a conservative parameter range.

Strategies using either 'ring' (also termed 'belt' or 'unifocal') electrode configurations [36, 37, 42, 43], scaling bipolar electrode size [30] or increasing number of electrodes [37, 44] have previously been investigated to address concerns about TCS spatial focality (and related stimulation current threshold). Here we further consider optimizing the shape (geometry) and number of electrodes. In addition, we develop 'modulation maps' addressing cellular target orientation. We compare the focality and efficacy of TCS stimulation of cortex with remotely spaced bipolar electrodes ('distant-bipolar') [6, 7, 11, 22, 28, 29], proximal bipolar electrodes ('adjacent-bipolar') [36–38], 'tripolar' electrodes and three ring electrode configurations: 'belt' [36, 37], 'concentric ring' and 'double concentric ring' using a finite element concentric sphere head model. The analysis of the electric field distributions induced inside the brain for different electrode configurations/geometries will allow for the 'rational' [45] design of TCS research and clinical protocols.

Model methods and analysis

The head was simulated as a 3D inhomogeneous medium comprising concentric spheres; each sphere was homogeneous and isotropic. The concentric head model (three- and four-layer) is accepted for its quantitative agreement with a variety of general observations of the electroencephalogram and magnetoencephalogram [23, 36, 46–48] and has been experimentally validated for transcranial stimulation [47].

Four concentric spheres of 61.53 mm, 64.03 mm, 71.76 mm and 76.49 mm radii represent the brain tissue, the cerebrospinal fluid (CSF), the skull and the scalp, respectively; the dimensions of the head are based on a 26 year old male [46]. The electrical properties of the four layers of the model were assigned representative average values taken from standard sources [49–52]: (in units of S m^{-1}) scalp 0.465; skull 0.010; CSF 1.650 and brain 0.200.

Although a symmetric model is used, 10/20 EEG notation is applied to indicate relative electrode location for different stimulation configurations. For distant-bipolar stimulation and double concentric ring, the electrodes were placed at equivalent distances from the head apex (analogous to Cz), while for all the other stimulation scenarios, the electrodes were oriented in order to obtain a peak electric field under the head apex.

We simulated a range of electrode configurations (indexed below); for several configurations we tested a subset of electrode geometries (e.g. size) as indicated. For existing clinical electrode configurations, studies with comparable placements are referenced.

(1) 'Distant-bipolar': Simulation with two disc electrodes placed 52.4 mm apart (center to center distance) to approximate standard tDCS stimulation of the primary motor cortex with the active electrode over C3 and the reference electrode at the forehead above the contralateral orbita [11, 22] (analogous electrode placements can be used according to the desired target). 'Distant-bipolar' is also referenced in the literature as unipolar stimulation [38].

(2) 'Adjacent-bipolar': Simulation with two disc electrodes separated by 25 mm. This is similar to the separation distance of electrodes previously referenced as 'bifocal stimulation' [36, 53].

(3) 'Tripolar': Simulation with three disc electrodes, each one separated by 25 mm from the other. This approximately corresponds to the first anode between CPz and Pz, second anode over C1 and the cathode over C2. The current at each anode was equal; the summed current at the single cathode was thus double of this value.

(4) 'Belt': Simulation with a cathode belt (2 mm wide, outer radius: 67 mm and inner radius: 65 mm) circling the forehead and an anode disc electrode placed on Cz. Belt stimulation is also referred to as 'unifocal stimulation' [36, 37].

(5) 'Concentric ring': Simulation with a cathode ring electrode (outer radius ranging 11–23 mm, inner radius: 9–21 mm) enclosing an anode disc electrode (of either 3 or 4 mm radius) over Cz.

(6) 'Double concentric ring': two concentric-ring electrodes: outer anode ring electrode (outer radius: 17/14 mm, inner radius: 15/13 mm); inner cathode ring electrode (outer radius: 11/9 mm, inner radius: 9/8 mm). Both the ring electrodes enclosed a third anode disc electrode (4 mm radius) over Cz. We considered both 'symmetric current', where the total current at each anode was equal, and 'asymmetric current', where the total current was different at each anode; in both cases, the current at the cathode was the summation of the two anodic currents.

Unless otherwise noted, all the disc electrodes had a default 4 mm radius [9, 54]. The thickness of the disc electrodes was 0.5 mm, while the ring electrode thickness varied from 0.25 mm to 2 mm; the thickness of the electrodes increased with increasing radius in order to maintain continuous contact with the curved scalp. Note that electrodes were only energized on the flat distal surface (see below) [55]. We do not explicitly consider the use of conductive gels or sponges.

The electrodes were modelled as conductors with the conductivity of copper (5.8×10^7 S m^{-1}). The Laplace equation $\nabla \cdot (\sigma \nabla V) = 0$ (V: potential; σ: conductivity) was solved and the boundary conditions used were (1) inward current flow $= J_n$ (normal current density) applied to the distal surface of the 'anode' electrode(s), (2) ground applied to the distal surface of the effective 'cathode' electrode and (3) all other external surfaces treated as insulated. Note that the total current at the effective cathode electrode thus equals the total anodic current; we confirmed similar current density profiles at the electrode/scalp interface of bipolar anode and cathode electrodes. Any current density inhomogeneities at the electrode/scalp interface are not reflected at the cortical surface due to the resistance of the skull [56] and did not affect the peak cortical electric field (see tolerance below).

For 'distance-bipolar' configuration stimulation, the total injected current was 1 mA (comparable to tDCS protocols); this resulted in a 0.328 V m^{-1} peak electric field, 1 mm under the cortical surface. For all other configurations the 'equivalent' total injected current (I_{eq}) was adjusted to obtain a 0.328 V m^{-1} peak electric field, 1 mm under the cortical surface.

The FEM solver was implemented using FEMLAB 3.3 (COMSOL Inc., Burlington, MA). The model was adaptively meshed into more than both 1,200,000 tetrahedral elements and 150,000 boundary triangular elements for each of the simulations. The linear system solver of conjugate gradients was used with a relative tolerance of 1×10^{-6}. Increasing the number of elements by a factor of 4 or reducing the relative tolerance of the solver to 1×10^{-8} changed the peak electric field values by less than 1%.

'Surface-magnitude' plots were generated by plotting the magnitude electric field 1 mm below the top half of the innermost sphere in the model (i.e. the brain surface). Cortical electric fields produced during surface stimulation have components both parallel and perpendicular to the head surface [36]. 'Surface-radial' plots were thus generated by plotting the component of the electric field on the brain surface in the direction normal to the surface (towards the sphere centre). 'Surface-radial $\pm$' plots further considered directionality (away or towards the cortical surface). 'Surface-tangential' plots were generated by plotting the component of the electric field parallel to the brain surface. 'Cross-section magnitude' plots were generated by plotting the magnitude electric field on a coronal slice through the sphere centre including the head apex. 'Cross-section radial' and 'cross-section tangential' plots represent electric fields oriented normal and parallel to the cortical surface, respectively. In the case of 'bipolar' stimulation, the coronal slice included

both electrode centres. In the case of 'tripolar' simulation, the coronal slice included the centre of the cathode and one of the anodes. In the case of ring configurations, fields were radially symmetric around the head apex. In addition for each of the electrode configurations, electric field magnitude line plots along the cortical surface and the brain depth were generated.

Results

For each configuration/geometry, we calculated the induced electric fields in the head. To allow direct comparison between configurations/geometries we applied 'equivalent currents' (I_{eq}) such that the peak cortical electric field in all cases was 0.328 V m^{-1} (table 1). The 'surface magnitude' and 'cross-section magnitude' plots of each configuration thus allow a direct comparison of relative spatial focality (figure 1). In addition, spatial space constants, quantifying surface and depth focality, are compared (table 1). For cortical surface/cross-section plots, radially oriented fields (normal to the brain surface) and tangential-oriented fields (along the brain surface) are considered independently (figure 1); note that in these plots the maximal radial and tangential fields are not the same, reflecting that the different configuration results in different ratios of radial and tangential currents. Finally for radial cortical fields, the direction of current flow is considered explicitly (surface-radial $\pm$ plots); these plots are normalized to the maximal positive and/or negative radial field to illustrate the relative bi-directionality of modulation. 'Unidirectional' modulation refers to electrode configurations with significant radial electric fields crossing the cortical surface in only one direction (i.e. with the return path sufficiently diffuse).

For all configurations the high resistivity of the skull relative to the scalp results in current 'shunting' through the scalp, consistent with previous transcranial stimulation studies [36–38]. The degree of shunting and the ratio of distal electrode-surface current density (mDESCD) with the peak cortical surface current density (CSCD) vary significantly across electrode configurations (table 1) [60]. As expected, I_{eq} scales directly with mDESCD/CSCD times minimum electrode area.

Disc configurations

'Distant-bipolar' stimulation results in relatively diffuse cortical and depth modulation (table 1, figure 2). The current crosses the cortex under each electrode and then transverses the brain resulting in *radial* fields under each electrode, and *tangential* fields in between (figure 1). The peak inward and outward radial currents are equivalent, resulting in bi-directional modulation.

Increasing the proximity of the two bipolar electrodes, 'adjacent-bipolar stimulation', results in more current being 'shunted' across the scalp surface. The equivalent current, to generate comparable peak cortical electric fields, is thus increased from 1 to 1.43 mA (table 1). In addition, though radial bi-directional currents are still prominent under each electrode, more relative tangential cortical fields are generated (figure 1). Thus for adjacent-bipolar stimulation the peak

Table 1. Summary of evaluated electrode configuration/geometries equivalent currents and focality.

Electrode configuration/geometry (all dimensions in mm)			$I_{\text{equivalent}}$ (mA)	Surface space constant (mm)	Depth space constant (mm)	DESCD (mA cm^{-2})	mDESCD/ CSCD
Bipolar							
disc electrode separation							
52.4 (distant bipolar)			1.00	22.90	13.60	1.99	302
25.0 (adjacent bipolar)			1.43	22.48	7.42	2.84	430
Tripolar							
disc electrode separation							
25			0.81/0.81/1.62	18.14	7.38	1.61/1.61/3.22	488
Concentric ring							
ring (o.r., i.r.)		*Disc (radius)*					
11, 9		4	8.12	8.89	3.25	6.46/16.15	2447
17, 15		4	3.71	10.61	3.80	1.84/7.38	1118
23, 21		4	2.45	12.58	4.58	0.89/4.87	738
67, 65 (Belt)		4	0.97	22.51	10.93	0.12/1.93	292
11, 9		3	7.59	8.81	3.20	6.04/26.84	4067
17, 15		3	3.49	10.52	3.76	1.73/12.34	1870
23, 21		3	2.41	12.42	4.42	0.87/8.52	1291
Double concentric ring							
outer ring	*inner ring*	*Disc (radius)*					
(o.r., i.r.)	*(o.r., i.r.)*						
14, 13	9, 8	4	29.92/59.84/29.92	8.65	8.72	35.27/112.05/59.52	16977
17, 15	11, 9	4	28.67/57.34/28.67	9.56	10.06	4.26/45.63/57.04	8642
67, 65	17, 15	4	2.10/4.20/2.10	28.80	23.26	0.25/2.09/4.18	633
17, 15	11, 9	–	7.30/7.30/0[a]	12.67	4.48	3.63/5.81/0	880
14, 13	9, 8	4	8.99/9.59/0.60[a]	11.72	4.12	0.60/17.96/1.19	2721
17, 15	11, 9	4	7.83/8.43/0.60[a]	12.85	4.60	3.89/6.71/1.19	1017
67, 65	17, 15	4	2.25/5.67/3.42[a]	28.86	23.27	0.27/2.82/6.80	1030

[a] Asymmetric current at anodes.

For each electrode configuration and geometry evaluated, the equivalent current (I_{eq}) corresponding to the total *surface* electrode current required to produce a 0.328 mV mm^{-1} field, 1 mm below the cortical surface, was determined. For each configuration the surface-space constants were determined, corresponding to the distance from the location of the peak electric field along the brain surface, to where the field decreased to 0.207 mV mm^{-1} (63.21% of peak). The depth-space constants were determined, corresponding to the distance from the cortical apex towards the brain centre, where the field decreased to 63.21% of its value at the apex. The distal electrode-surface current density (DESCD: total current/area) for all configurations is also indicated. Note that the current density 1 mm below the cortical surface (CSCD) is 0.0066 mA cm^{-2} for all cases due to use of I_{eq}. For the mDESCD/CSCD ratio (rounded to the next significant integer), maximal values of DESCD were considered. These indicators provide only broad pointers of how efficient each configuration is in guiding the current into the brain (as opposed to along the scalp surface) and localizing stimulation to superficial cortical regions. For any given application, these metrics may not necessarily indicate increased efficacy of safety (see the Discussion section). (Note: 'o.r.', 'i.r.', 'DESCD' and 'CSCD' refer to 'ring outer radius', 'ring inner radius', 'distal electrode-surface current density' and 'cortical surface current density', respectively).

electric field is between both electrodes, while the peak radial field is under each electrode. Consistent with previous studies [36, 38], we found that 'adjacent-bipolar' stimulation is more focal, along both the cortical surface and the depth, than 'distant-bipolar' stimulation (figure 2) at the cost of the shunted scalp current.

The 'tripolar' configuration effectively divides the anodic current into two electrodes (0.81 mA equivalent current at two anodes and −1.62 mA at the effective cathode). Tripolar stimulation was found to have similar total magnitude field focality as 'adjacent-bipolar' stimulation (table 1, figure 2), but directional surface plots indicate that while radial currents dominate under the single cathode, tangential currents are prominent under the two anodes (figure 1).

Ring configurations

Although the 'belt' configuration is not evidently more focal than 'distant-bipolar' stimulation (figures 1 and 2), it requires

slightly less equivalent current (0.97 mA). A relatively high density radial current crosses the brain surface under the centre disc electrode; the return current path to the belt electrode is relatively diffuse. The net result is unidirectional and radial modulation under the centre disc.

The 'concentric-ring' configuration had the highest relative focality of the configurations evaluated (table 1, figure 2) at the cost of the moderately increased equivalent current (3.71 mA). Similar to belt stimulation, fields were dominantly radial under the disc electrode and unidirectional (figure 1). In the case of the concentric ring, the current crosses the brain at high current density under the disc and rapidly diffuses in the brain (diffuse current densities producing negligible electric fields); the current remains diffuse as it exits the brain and returns to the ring electrode via the scalp. The increased equivalent current presumably reflects the portion of the current that 'shunts' between the disc and ring electrode along the scalp *without* crossing the brain (without effecting brain function, see the Discussion section). Increasing the ring
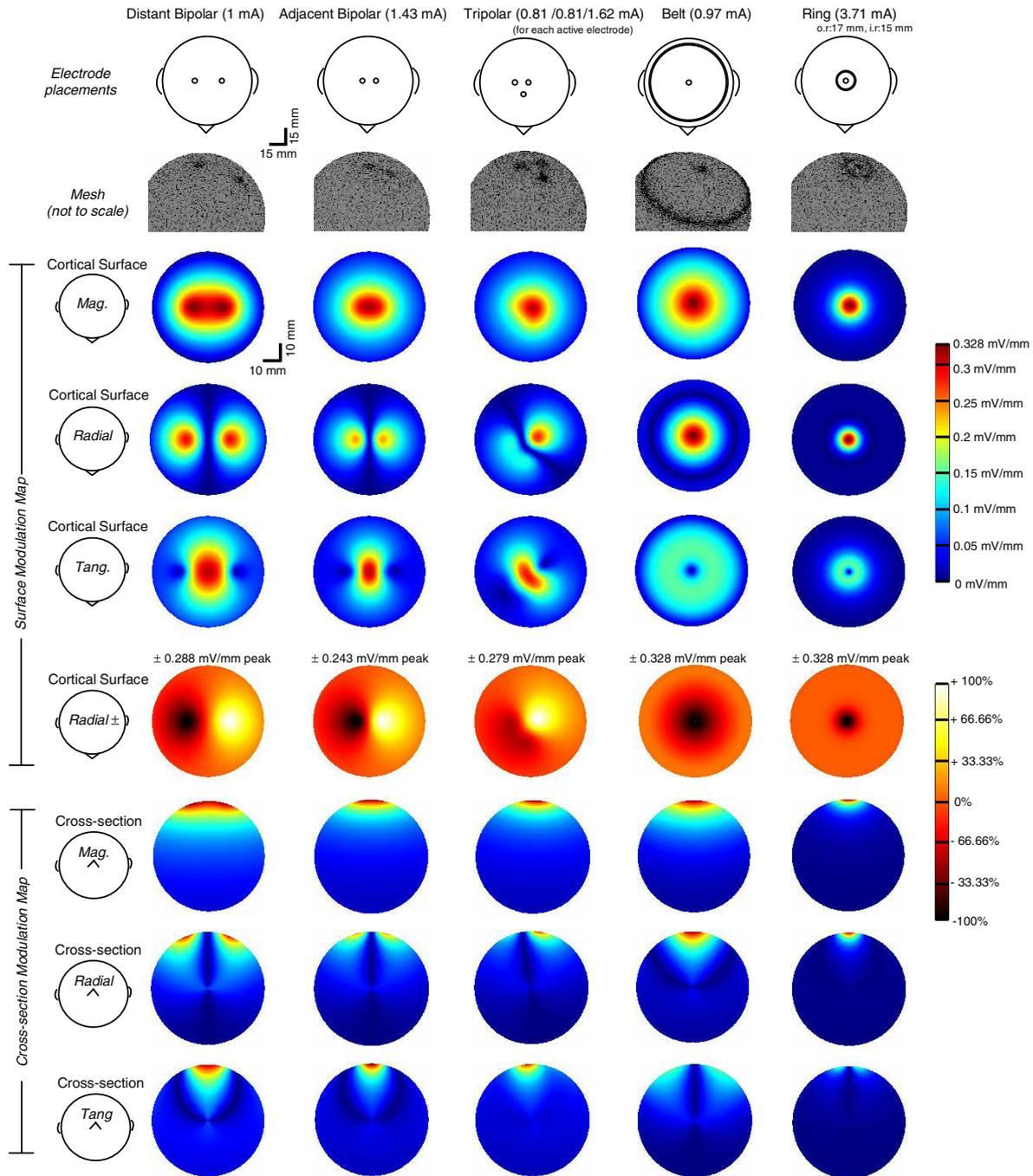
Figure 1. Finite element model of brain electric fields induced by varied surface stimulation electrode configurations. For the five electrode configurations illustrated (left to right) the total electrode current (I_{eq}) was adjusted to produce a 0.328 mV mm^{-1} peak electric field, 1 mm below the cortical surface. The top two rows diagram the *electrode geometries* and *solver mesh*. The remaining rows plot the induced electric fields in varied planes and directions (see the 'Model methods and analysis' section). The *surface-magnitude* plot maps the electric field magnitude along the top head hemisphere, 1 mm below the cortical surface. The *surface-radial* and *surface-tangential* plots decompose this plot into the radial (normal to the surface) and tangential (along the brain surface) directions; note that in the cases of bipolar stimulation and tripolar stimulation significant differences exist between the surface-magnitude and surface-directional (radial and tangential) plots, while in the belt and ring configurations the surface magnitude and surface radial are similar, consistent with dominantly radial surface cortical current flow. The *surface-radial* ± plots are normalized to the respective peak surface-radial field (indicated in the inset) and highlight which configurations produce radial bi-directional modulation. The *cross-section magnitude* plot maps the electric field magnitude on a central cortical cross-section (see the 'Model methods and analysis' section). The *cross-section-radial* and *cross-section-tangential* plots decompose this plot into the radial (normal to the surface) and tangential (along the brain surface) directions. All surface/cross-section electric field plots are on the indicated spatial scale; the mesh diagrams are scaled for clarity. (Note: 'o.r.', 'i.r.', 'Mag' and 'Tang' refer to 'ring outer radius', 'ring inner radius', 'magnitude' and 'tangential', respectively.)
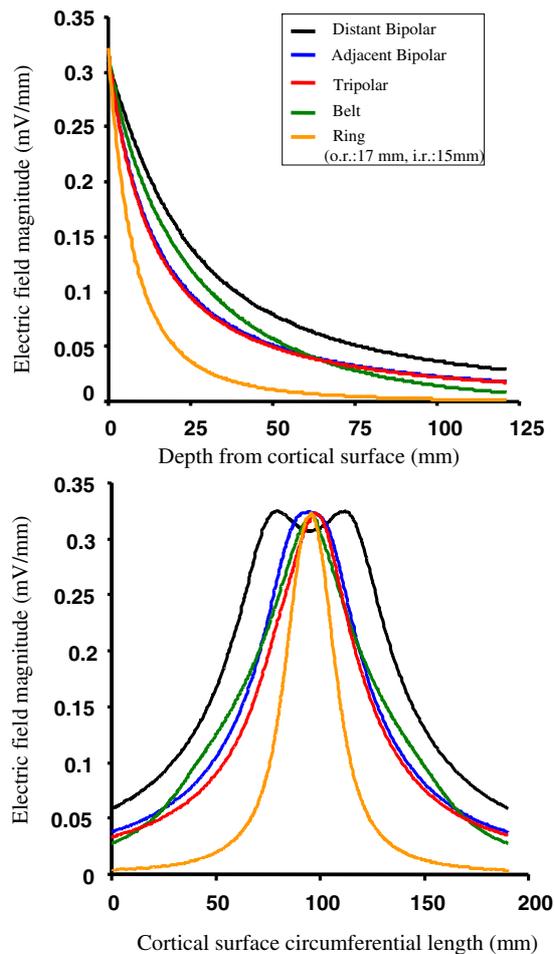
Figure 2. Electric field profiles along the cortical surface and brain depth induced by varied surface stimulation electrode configurations. For the five electrode configurations illustrated in figure 1, the line plots of electric field magnitude along the cortical surface midline and down the brain cross-section midline are overlaid. Note that the equivalent current for each configuration has been adjusted (I_{eq}) to produce a 0.328 mV mm^{-1} peak electric field, 1 mm under the cortical surface. The peak electric field in all configurations is at the head apex except for distant-bipolar where two peaks are observed corresponding to the two stimulation sites. (Note: 'o.r.' and 'i.r.' refer to 'ring outer radius' and 'ring inner radius', respectively.)

diameter decreases the shunt fraction and thus the required equivalent current, at the cost of focality (table 1).

For moderate ring diameters, electric fields distribution using the 'double concentric-ring' configuration roughly approximated those generated under the concentric ring (figure 1), with the cortical radial stimulation area increasing and I_{eq} decreasing with increasing outer ring diameter. Appropriate selection of ring diameters and/or use of asymmetric currents (where the total anodic current at the inner disc and that at the outer ring are not equal) resulted in the generation of ring modulation regions (figure 3). Similarly, the relative balance of the radial versus tangential electric field can be controlled. Rather than suggesting specific clinical applications, these examples illustrate how electrode number,

size and current balance can be independently controlled in designing stimulation configurations.

Discussion

Precision of a reduced head model

The accuracy of any given stimulation model is restricted by the calculation of accurate voltage profiles and the subsequent prediction of relevant 'modulation' regions from these voltage profiles. The former is limited by the level of inhomogeneity and anisotropy modeled. The advantages of using a reduced concentric-sphere head model for this initial evaluation include the ability to directly compare different configurations/geometries without concomitant complexity related to head asymmetry. Improving the precision of the head model will enhance the accuracy of the electric field calculations, including the incorporation of anatomical information from individual MRI scans [3, 57, 58] and conductivity data derived from diffusion tensor imaging (DT-MRI) [59]. We note that our distant-bipolar calculations are in general agreement with previous tDCS stimulations using concentric spheres [56] and MRI-based anatomy [60]. The results reported here using the optimized electrode configurations thus represent an important 'proof-of-principle' supporting further characterization.

Cortical modulation functions (maps): representation of relevant modulation regions

Transcranial stimulation generates extracellular voltage gradients (electric fields) inside the head, and these fields will lead to the polarization of sections of the neuronal membrane. This induced membrane polarization will affect a range of functional/cellular properties. Relatively strong supra-threshold electric fields will trigger action potentials. Sub-threshold fields can modulate the firing properties of neurons (e.g. action potential threshold/timing [34, 61]), synaptic efficacy [33] and neuronal information processing [35, 62]. It is important to note that in response to any electric field, different compartments of the same neuron will simultaneously either depolarize or hyperpolarize [61–63]. Thus the complex 'modulation' by electric stimulation cannot necessarily be explained by a simple 'increase' or 'decrease' in excitability.

It is well established that the 'point' extracellular voltage generated by applied stimulation does not provide a useful indication of neuronal modulation; for this reason proximity to anode or cathode does not necessarily provide meaningful information on cell modulation. Rather, the *spatial distribution* of extracellular voltages (electric field) is applied to a modulation function (which may also include information on neuronal geometry, membrane biophysics and synaptic properties) that determines neuronal modulation at each location. The classic 'activating function' considers the electric field *derivative* along each membrane segment [48, 64–66].

In determining 'cortical modulation functions' in this report, we considered the electric field magnitude induced in
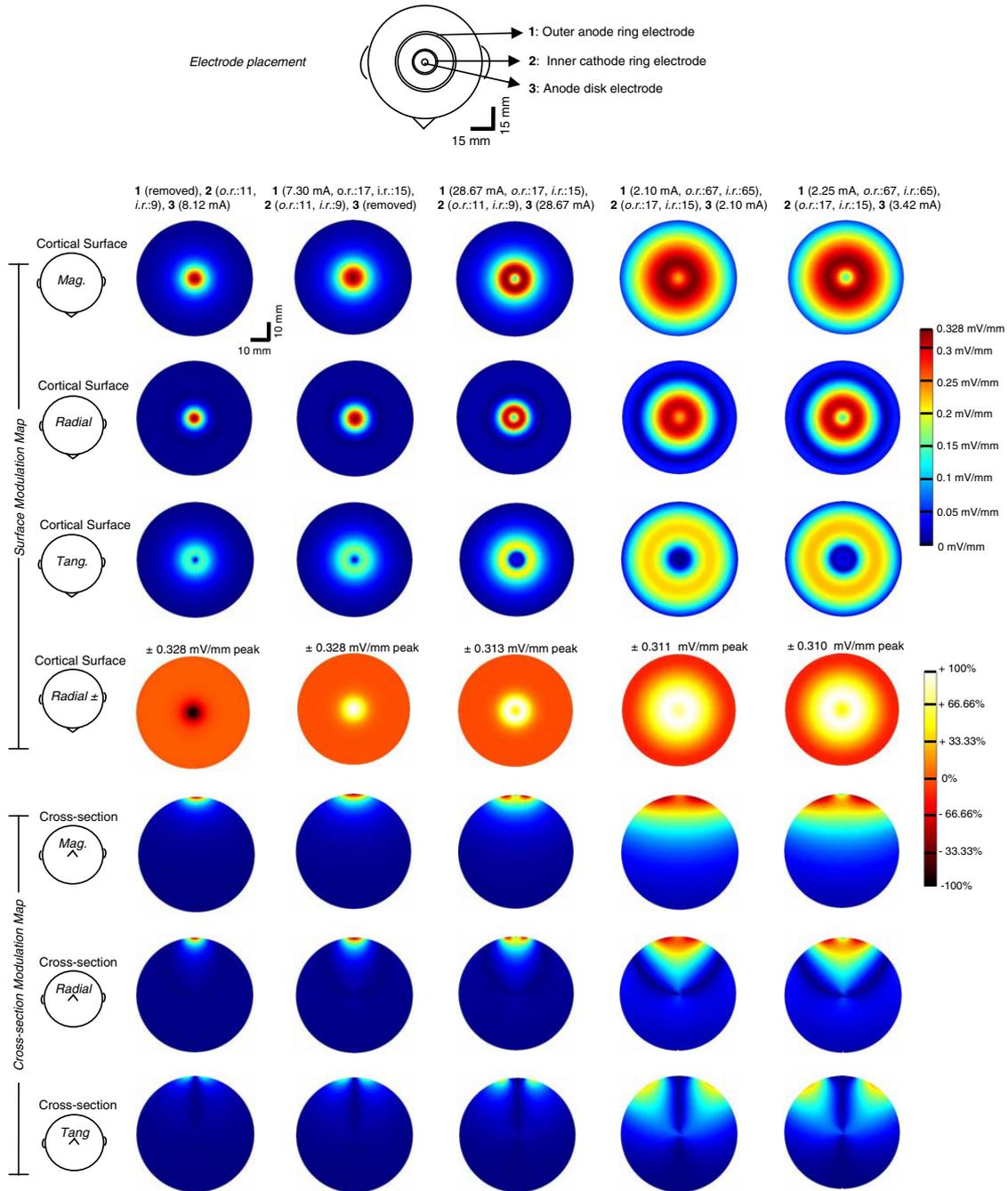
Figure 3. Finite element model of brain electric fields induced by double concentric-ring stimulation electrode configurations. For the double concentric-ring configuration, we considered energizing either only two electrodes (with one electrode insulated/removed) or energizing all electrodes ('tripolar' modulation at two ring electrode geometries). For the five conditions illustrated, the total electrode current (I_{eq}) was adjusted to produce a 0.328 mV mm^{-1} peak field, 1 mm below the cortical surface. The top row diagrams the electrode configuration; the ring electrode radii and current was varied. The inner ring was energized as the only cathode and the disc electrode had 4 mm radius in all cases. The remaining rows plot the induced electric fields in varied planes and directions. For each case, neuronal modulation was represented using *surface-magnitude*, *surface-radial, surface-tangential, surface-radial ±, cross-section magnitude*, *cross-section-radial* and *cross-section-tangential* (see the 'Model methods and analysis' section). Column 1: energizing only the central disc electrode and the inner ring (ring 2) duplicates the single concentric-ring configuration. Column 2: energizing only the two ring electrodes results in dominantly radial modulation under the rings. Columns 3 and 4: energizing all electrodes (with total anodic current at the centre disc and outer ring matched) resulted in a modulation 'ring' that scaled with electrode size, surrounding a centred un-stimulated region. Column 5: asymmetric current at each anode resulted in a more distinct ring modulation region. Note that the relatively high I_{eq} for double concentric rings results from significant skull/scalp shunting but that the peak brain electric field (and hence current density) is normalized across all cases. All surface/cross-section electric field plots are on the indicated spatial scale. All dimensions are in mm. (Note: 'o.r.', 'i.r.', 'Mag' and 'Tang' refer to 'ring outer radius', 'ring inner radius', 'magnitude' and 'tangential', respectively.)

the brain ('surface-magnitude' and 'cross-section magnitude' plots/space constants) and the cortical electric field in either the radial ('surface-radial'/'cross-section radial' plot) or tangential ('surface-tangential'/'cross-section tangential' plot) directions. The consideration of electric field (as opposed to the electric field derivative/classical activating function [67–69]) may be a suitable approximation if for transcranial current stimulation, the induced electric field is locally uniform on the scale of any given neuron (figure 1) [56, 60] and neuronal modulation is directly related to uniform electric field amplitude. The latter is supported by experimental and theoretical studies showing that (1) the polarization of short or bent cortical axons is linear with (sub-threshold) electric field amplitude [67, 70–74]; (2) synaptic efficacy is quasi-linear with electric field amplitude [33, 61]; (3) somatic and dendritic process polarization is linear with (sub-threshold) uniform electric field amplitude [33, 75–77] and (4) metrics of neuronal excitability vary with electric field amplitude [33, 61, 74, 78–85].

The above reports also reinforce that uniform electric fields preferentially polarize neuronal structures oriented parallel to the direction of the field. Whereas our magnitude plots assume no coherent neuronal geometry, radial and tangential plots represent modulation of cortical structures oriented preferentially normal to the cortical surface (e.g. superficial cortical pyramidal neurons) or parallel to the surface (e.g. axons of passage, deeper cortical neurons), respectively [86, 87]. For example, based on animal studies [27, 32] and simulations [64], inwardly directed radial fields under anodes would be expected to depolarize the soma and simultaneously hyperpolarize the apical dendrites of superficial (hence radially oriented) primary cortical neurons (surface-radial ± plots, figures 1 and 3).

Consistent with previous studies, we found that maximal *magnitude* electric fields were observed in the cortical regions under *and* between electrodes. However, we report that the consideration of the specific electric field direction (structure orientation) changes the modulation profile. For example, the surface-radial electric field (presumably superficial cortical pyramids) modulation region for bipolar stimulation restricts modulation to *only* regions under the electrodes (between electrodes the electric field is tangential); this is consistent with clinical observations that neuronal modulation is restricted to regions under electrodes [30]. Similarly, consideration of surface-radial electric fields further enhances the efficacy of the belt configuration relative to the adjacent-bipolar configuration (belt: 0.328 mV mm^{-1} radial field per 0.97 mA; adjacent-bipolar 0.243 mV mm^{-1} radial field per 1.43 mA), consistent with clinical observations [37]. Electric field orientation-specific modulation maps (figure 1) may thus provide practical clinical guidelines not apparent from magnitude plots.

Interestingly, the tripolar configuration produces the distinct radial modulation region and tangentially modulated regions. This configuration may thus be used to probe the functional/therapeutic significance of sub-threshold tangential electric fields.

Ring configurations generally favour surface radial modulation. For belt, concentric-ring and double concentric-ring configurations, the similarity between surface-magnitude and surface-radial plots (reflecting relatively small tangential currents) reduces ambiguity on appropriate modulation representation. In addition, surface-radial ± plots illustrate that with these circular configurations, bi-directional modulation effects are avoided.

Our cortical modulation maps do not explicitly consider neuronal geometry inhomogeneity, which would require complex reproduction of cortical gyri and sulci, as well as neuronal (cortical layer) sub-types. The assumption that superficial cortical neurons, located at gyri crowns, are preferentially modulated is consistent with the rapid decay in field intensity with cortical depth (figure 1 *Cross-sections*, table 1). Our surface cortical modulation maps (1 mm below the cortical surface; figure 1) may thus, to a first approximation, predict stimulation effects on these relatively homogenous oriented superficial cortical neurons. Indeed, our results with the bipolar configuration are consistent with clinical observations (see above), and the general clinical finding that the anodal/cathodal field induces reliable and distinct effects supports a relatively homogenous target neuronal population. Nonetheless, the predictions made in this study, regarding optimized electrode configurations and orientated-modulation maps, should be experimentally verified [30] and corroborated with anatomically detailed models.

Since the static field approximation [48] in our model implies linearity of the electric field solution, our induced electric field spatial profile results can be extrapolated to a wide range of stimulation waveforms (e.g. pulsed or AC fields [1–5, 31]) and scale linearly with stimulation magnitude (e.g. 260 μA–2 mA tDCS and >350 mA TES [37]). However, the induced electric field magnitude (e.g. sub/supra-threshold stimulation) and temporal waveform (e.g. frequency) will affect the appropriate modulation function [35, 88–90] and the accuracy of our simplified (locally uniform) electric field-based modulation maps.

Optimization of electrode configuration/geometry: efficacy and safety

The optimal electrode configuration/geometry will depend on the TCS application. However, spatial focality, cellular type specificity and control of bi-directional modulation at return electrodes are generally desired. As a rule, increasing the distance between stimulation electrodes (or equivalently increasing ring diameter) decreases the current portion shunted through the skull/scalp and increases the relative current crossing the brain (table 1, $I_{equivalent}$ and mDESCD/CSCD), while reducing spatial focality (table 1, surface and depth space constant). Placing electrodes proximal to each other increases focality at the expense of the total equivalent current (to obtain comparable efficacy with remote electrodes). Thus, when comparing electrode configurations, increased electrode current or electrode current density does not necessarily equate with increased brain modulation (cortical electric fields).

Concerns about TCS safety generally focus on the total electrode current, electrode-surface current density (current/area), total charge (current × stimulation duration) or total charge density (total charge/electrode area) [39, 40, 92].

We note that the (charge-related) electrochemical product may not be an issue for acute noninvasive stimulation [93] and that the magnitude of scalp sensation does not correlate with threshold of brain stimulation [40, 44]. Here we propose a supplementary safety consideration of a normalized peak cortical field, reportable as equivalent currents (I_{eq}) to a 'standard' configuration (1 mA, distant-bipolar). Rational stimulation design may balance scalp current density and equivalent current (cortical electric field) factors (table 1). Nitsche *et al* [30] demonstrated that during tDCS bipolar stimulation with different size square electrodes, calculated electrode-surface current density (1 mA 35 cm^{-2}) roughly standardizes cortical response. Standardization to calculated electrode-surface current density (total current/electrode area) assumes that the current density at the scalp scales consistently with the current density at the brain; this assumption does not necessarily hold across electrode configurations (table 1, in part because of differences in fractional scalp/skull loss) or for relatively small electrodes. For example, a micro-electrode (0.01 cm^2 area) with 'standardized' current density (1 mA/ 35 cm$^2 \times$ 0.01 cm^2 = 0.0003 mA current) will not be effective. In addition, current density is not uniform on the electrode surface [56]. Nonetheless, approximated uniform electrode-surface current density (total current/electrode area) remains a useful functional/safety metric because it presumably places an upper limit on current density, and hence electric field in the brain; assuming current density diffusion through skull [23, 36, 38, 48, 60] offsets current density concentration at the electrode edges [56].

For any given application and temporal waveform (e.g. tDCS for depression, ECT for depression, CES for pain), an appropriate I_{eq} multiplying factor can be determined (desired theraputic peak cortical electric field in mV mm^{-1}/0.328 mV mm^{-1}). For a *given therapy and temporal waveform*, the I_{eq} multiple factor should be kept constant when changing electrode positions/configuration in order to elicit similar peak cortical fields thus maintaining efficacy; however I_{eq} will vary with electrode configuration and hence so will the total applied current. For this reason when changing configurations, maintaining the total applied current (electrode current density, electrode charge) may not be appropriate. Since the spatial profile of the induced electric field is independent of waveform and application, the *relative* spatial focality of different electrode configurations may be directly compared by normalizing to the peak cortical electric field (using I_{eq}), and the resultant directional modulation maps generated in this way can be used to predict relative structural targeting (figures 1 and 3). I_{eq} has a further advantage of indicating relative shunting across electrode configurations (more robustly than mDESCD/CSCD).

TES and electroconvulsive therapy both have electrode-surface current densities significantly exceeding 1 mA cm^{-2} and apply currents $>100 \times I_{eq}$ [5, 37]. However, because of the difference in stimulation waveform (e.g. number of pulses) and desired clinical outcome, efficacy and safety considerations for TES and electroconvulsive therapy are fundamentally different. The I_{eq} multiple does not in itself define stimulation effects, without explicit consideration of waveform and therapy factors.

Approaches using multiple electrodes and varying electrode geometries have been well characterized for peripheral nerve stimulation [94]. Concentric-ring electrode configurations (consisting of a centre electrode surrounded by a ring electrode) and ring electrodes have been previously used for peripheral nerve/muscle fibre stimulation [65], producing anaesthetic effects [95] and seizure control [43]. Analytical solutions for concentric-ring stimulation of homogenous tissue have been proposed [42]. The mathematically complimentary principle of using ring electrodes to improve the spatial focality of bio-potential recording has been applied for EEG [96], EMG [97] and ECG [98] signals. Our results indicate that the focality of clinical TCS stimulation, targeting radially oriented superficial structures, can be markedly increased by appropriate application of concentric-ring stimulation electrodes.

In summary, control of surface electrode geometry (shape and number) will modulate both the structural specificity and spatial focality of TCS stimulation. Optimization of focality must be balanced against the increased electrode current density and scalp/skull current (which may not necessarily reflect safety concerns). The configurations explicitly considered in this report can be combined and indeed serve only to illustrate principles of design. Our results thus support the further development of TCS technology incorporating rationally designed [45] target-specific (pathology, structure) electrode configurations.

Acknowledgments

References

[1] Zentner J 1989 Noninvasive motor evoked potential monitoring during neurosurgical operations on the spinal cord *Neurosurgery* **24** 709–12

[2] Calancie B, Harris W, Broton J G, Alexeeva N and Green B A 1998 'Threshold-level' multipulse transcranial electrical stimulation of motor cortex for intraoperative monitoring of spinal motor tracts: description of method and comparison to somatosensory evoked potential monitoring *J. Neurosurg.* **88** 457–70

[3] Holdefer R N, Sadleir R and Russell M J 2006 Predicted current densities in the brain during transcranial electrical stimulation *Clin. Neurophysiol.* **117** 1388–97

[4] Schroeder M J and Barr R E 2001 Quantitative analysis of the electroencephalogram during cranial electrotherapy stimulation *Clin. Neurophysiol.* **112** 2075–83

[5] Nadeem M, Thorlin T, Gandhi O P and Persson M 2003 Computation of electric and magnetic stimulation in human head using the 3-D impedance method *IEEE Trans. Biomed. Eng.* **50** 900–7

[6] Nitsche M A and Paulus W 2001 Sustained excitability elevations induced by transcranial DC motor cortex stimulation in humans *Neurology* **57** 1899–901

[7] Nitsche M A, Nitsche M S, Klein C C, Tergau F, Rothwell J C and Paulus W 2003 Level of action of cathodal DC polarisation induced inhibition of the human motor cortex *Clin. Neurophysiol.* **114** 600–4

[8] Ardolino G, Bossi B, Barbieri S and Priori A 2005 Non-synaptic mechanisms underlie the after-effects of cathodal transcutaneous direct current stimulation of the human brain *J. Physiol.* **568** 653–63

[9] Marshall L, Molle M, Siebner H R and Born J 2005 Bifrontal transcranial direct current stimulation slows reaction time in a working memory task *BMC Neurosci.* **6** 23

[10] Iyer M B, Mattu U, Grafman J, Lomarev M, Sato S and Wassermann E M 2005 Safety and cognitive effect of frontal DC brain polarization in healthy individuals *Neurology* **64** 872–5

[11] Nitsche M A, Schauenburg A, Lang N, Liebetanz D, Exner C, Paulus W and Tergau F 2003 Facilitation of implicit motor learning by weak transcranial direct current stimulation of the primary motor cortex in the human *J. Cogn. Neurosci.* **15** 619–26

[12] Antal A, Nitsche M A, Kincses T Z, Kruse W, Hoffmann K P and Paulus W 2004 Facilitation of visuo-motor learning by transcranial direct current stimulation of the motor and extrastriate visual areas in humans *Eur. J. Neurosci.* **19** 2888–92

[13] Uy J and Ridding M C 2003 Increased cortical excitability induced by transcranial DC and peripheral nerve stimulation *J. Neurosci. Methods* **127** 193–7

[14] Kincses T Z, Antal A, Nitsche M A, Bartfai O and Paulus W 2004 Facilitation of probabilistic classification learning by transcranial direct current stimulation of the prefrontal cortex in the human *Neuropsychologia* **42** 113–7

[15] Fregni F *et al* 2005 Anodal transcranial direct current stimulation of prefrontal cortex enhances working memory *Exp. Brain Res.* **166** 23–30

[16] Boggio P S, Bermpohl F, Vergara A O, Muniz A L, Nahas F H, Leme P B, Rigonatti S P and Fregni F 2006 Go-no-go task performance improvement after anodal transcranial DC stimulation of the left dorsolateral prefrontal cortex in major depression *J Affect. Disord.* **101** 91–8

[17] Lisanby S H 2007 Electroconvulsive therapy for depression *N. Engl. J. Med.* **357** 1939–45

[18] Webster B R, Celnik P A and Cohen L G 2006 Noninvasive brain stimulation in stroke rehabilitation *NeuroRx.* **3** 474–81

[19] Liebetanz D, Klinker F, Hering D, Koch R, Nitsche M A, Potschka H, Loscher W, Paulus W and Tergau F 2006 Anticonvulsant effects of transcranial direct-current stimulation (tDCS) in the rat cortical ramp model of focal epilepsy *Epilepsia* **47** 1216–24

[20] Boggio P S, Ferrucci R, Rigonatti S P, Covre P, Nitsche M A, Pacual-Leone A and Fregni F 2006 Effects of transcranial direct current stimulation on working memory in patients with parkinson's disease *J. Neurol. Sci.* **249** 31–8

[21] Fregni F *et al* 2006 A sham-controlled, phase II trial of transcranial direct current stimulation for the treatment of central pain in traumatic spinal cord Injury *Pain* **122** 197–209

[22] Nitsche M A *et al* 2005 Modulating parameters of excitability during and after transcranial direct current stimulation of the human motor cortex *J. Physiol.* **568** 291–303

[23] Suihko V 1998 Modeling direct activation of corticospinal axons using transcranial electrical stimulation *Electroencephalogr. Clin. Neurophysiol.* **109** 238–44

[24] Nitsche M A, Fricke K, Henschke U, Schlitterlau A, Liebetanz D, Lang N, Henning S, Tergau F and Paulus W 2003 Pharmacological modulation of cortical excitability

shifts induced by transcranial direct current stimulation in humans 2003 *J. Physiol.* **533.1** 293–301

[25] Liebetanz D, Nitsche M A, Tergau F and Paulus W 2002 Pharmacological approach to the mechanisms of transcranial DC- stimulation-induced after-effects of human motor cortex *Brain* **125** 2238–47

[26] Bindman L J, Lippold O C and Redfearn J W 1964 The action of brief polarizing currents on the cerebral cortex of the rat (1) during current flow and (2) in the production of long-lasting after-effects *J. Physiol.* **172** 369–82

[27] Purpura D P and McMurty J G 1965 Intracellular activities and evoked potential changes during polarization of motor cortex *J. Neurophysiol.* **28** 166–85

[28] Nitsche M A and Paulus W 2000 Excitability changes induced in the human motor cortex by weak transcranial direct current stimulation *J. Physiol.* **527** 633–9

[29] Lang N, Nitsche M A, Paulus W, Rothwell J C and Lemon R N 2004 Effects of transcranial direct current stimulation over the human motor cortex on corticospinal and transcallosal excitability *Exp. Brain Res.* **156** 439–43

[30] Nitsche M A, Doemkes S, Karakose T, Antal A, Liebetanz D, Lang N, Tergau F and Paulus W 2007 Shaping the effects of transcranial direct current stimulation of the human motor cortex *J. Neurophysiol.* **97** 3109–17

[31] Marshall L, Helgadóttir H, Mölle M and Born J 2006 Boosting slow oscillations during sleep potentiates memory *Nature* **444** 610–3

[32] Gartside I B 1968 Mechanisms of sustained increases of firing rate of neurons in the rat cerebral cortex after polarization: role of protein synthesis *Nature* **220** 383–4

[33] Bikson M, Inoue M, Akiyama H, Deans J K, Fox J E, Miyakawa H and Jefferys J G 2004 Effects of uniform extracellular DC electric fields on excitability in rat hippocampal slices in vitro *J. Physiol.* **557** 175–90

[34] Radman T, Su Y, An J H, Parra L C and Bikson M 2007 Spike timing amplifies the effect of electric fields on neurons: implications for endogenous field effects *J. Neurosci.* **27** 3030–6

[35] Deans J K, Powell A D and Jefferys J G 2007 Sensitivity of coherent oscillations in rat hippocampus to AC electric fields *J. Physiol.* **583** 555–65

[36] Saypol J M, Roth B J, Cohen L G and Hallett M 1991 A theoretical comparison of electric and magnetic stimulation of the brain *Ann. Biomed. Eng.* **19** 317–28

[37] Rossini P M, Marciani M G, Caamia M, Roma V and Zarola F 1985 Nervous propagation along 'central' motor pathways in intact man: characteristics of motor responses to 'bifocal' and 'unifocal' spine and scalp non-invasive stimulation *Electroencephalogr. Clin. Neurophysiol.* **61** 272–86

[38] Nathan S S, Sinha S R, Gordon B, Lesser R P and Thakor N V 1993 Determination of current density distributions generated by electrical stimulation of the human cerebral cortex *Electroencephalogr. Clin. Neurohysiol.* **86** 183–92

[39] Priori A 2003 Brain polarization in humans: a reappraisal of an old tool for prolonged non-invasive modulation of brain excitability *Clin. Neurophysiol.* **114** 589–95

[40] Nitsche M A, Liebetanz D, Lang N, Antal A, Tergau F and Paulus W 2003 Safety criteria for transcranial direct current stimulation (tDCS) in humans *Clin. Neurophysiol.* **114** 2220–2

[41] Priori A 2003 Reply to Dr. Paulus *Clin. Neurophysiol.* **114** 2223

[42] Van Oosterom A and Strackee J 1983 Computing the lead field of electrodes with axial symmetry *Med. Biol. Eng. Comput.* **21** 473–81

[43] Besio W G, Koka K and Cole A 2007 Effects of noninvasive transcutaneous electrical stimulation via concentric ring electrodes on pilocarpine-induced status epilepticus in rats *Epilepsia* **48** 2273–9

[44] Suihko V 2002 Modelling the response of scalp sensory receptors to transcranial electrical stimulation *Med. Biol. Eng. Comput.* **40** 395–401

[45] Bikson M, Radman T and Datta A 2006 Rational modulation of neuronal processing with applied electric Fields *Conf. Proc. IEEE Eng. Med. Biol. Soc.* **1** 1616–9

[46] Ferdjallah M, Bostick F X Jr and Barr R E 1996 Potential and current density distributions of cranial electrotherapy stimulation (CES) in a four-concentric-spheres model *IEEE Trans. Biomed. Eng.* **43** 939–43

[47] Rush S and Driscoll D A 1968 Current distribution in the brain from surface electrodes *Anesth. Analg.* **47** 717–23

[48] Stecker M M 2005 Transcranial electric stimulation of motor pathways: a theoretical analysis *Comput. Biol. Med.* **35** 133–55

[49] Geddes L A and Baker L E 1967 The specific resistance of biological material-a compendium of data for the biomedical engineer and physiologist *Med. Biol. Eng.* **5** 271–93

[50] Akthari *et al* 2002 Conductivities of three-layer live human skull *Brain Topogr.* **14** 151–67

[51] De Mercato G and Garcia Sanchez F J 1992 Correlation between low- frequency electric conductivity and permittivity in the diaphysis of bovine femoral bone *IEEE Trans. Biomed. Eng.* **39** 523–26

[52] Ranck J B 1963 Specific impedance of rabbit cerebral cortex *Exp. Neurol.* **7** 144–52

[53] Cohen L G and Hallett M 1988 Methodology for non-invasive mapping of human motor cortex with electrical stimulation *Electroencephalogr. Clin. Neurophysiol.* **69** 403–11

[54] Marshall L, Molle M, Hallschmid M and Born J 2004 Transcranial direct current stimulation during sleep improves declarative memory *J Neurosci.* **24** 9985–92

[55] Szmurlo R, Sawicki B, Starzynski J and Wincenciak S 2006 A comparison of two models of electrodes for ECT simulations *IEEE Trans. Magnet.* **42** 1395–8

[56] Miranda P C, Lomarev M and Hallet M 2006 Modeling the current distribution during transcranial direct current stimulation *Clin. Neurophsyiol.* **117** 1623–9

[57] De Lucia M, Parker G J, Embleton K, Newton J M and Walsh V 2007 Diffusion tensor MRI-based estimation of the influence of brain tissue anisotropy on the effects of transcranial magnetic stimulation *Neuroimage* **36** 1159–70

[58] Wagner T A, Zahn M, Grodzinsky A J and Pascual-Leone A 2004 Three-dimensional head model simulation of transcranial magnetic stimulation *IEEE Trans. Biomed. Eng.* **51** 1586–98

[59] McIntyre C C, Mori S, Sherman D L, Thakor N V and Vitek J L 2004 Electric field and stimulating influence generated by deep brain stimulation of the subthalamic nucleus *Clin. Neurophysiol.* **115** 589–95

[60] Wagner T, Fregni F, Fecteau S, Grodzinsky A, Zahn M and Pascual-Leone A 2007 Transcranial direct current stimulation: a computer based human model study *Neuroimage* **35** 1113–24

[61] Jefferys J G R 1981 Influence of electric fields on the excitability of granule cells in guinea-pig hippocampal slices *J. Physiol.* **319** 143–52

[62] Jefferys J G, Deans J, Bikson M and Fox J 2003 Effects of weak electric fields on the activity of neurons and neuronal networks *Radiat. Prot. Dosim.* **106** 321–3

[63] Ranck J B Jr 1975 Which elements are excited in electrical stimulation of mammalian central nervous system: a review *Brain Res.* **98** 417–40

[64] Rattay F 1986 Analysis of models for external stimulation of axons *IEEE Trans. Biomed. Eng.* **33** 974–7

[65] Rattay F 1989 Analysis of models for extracellular fiber stimulation *IEEE Trans. Biomed. Eng.* **36** 676–82

[66] Plonsey R and Barr R C 1995 Electric field stimulation of excitable tissue *IEEE Trans. Biomed. Eng.* **42** 329–36

[67] Tranchina D and Nicholson C 1986 A model for the polarization of neurons by extrinsically applied electric fields *J. Biophys.* **50** 1139–56

[68] Rattay F 1998 Analysis of the electrical excitation of CNS neurons *IEEE Trans. Biomed. Eng.* **45** 766–72

[69] McIntyre C C and Grill W M 1999 Excitation of central nervous system neurons by nonuniform electric fields *J. Biophys.* **76** 878–88

[70] Maccabee P J, Amassian V E, Eberle L P and Cracco R Q 1993 Magnetic coil stimulation of straight and bent amphibian and mammalian peripheral nerve in vitro: locus of excitation *J. Physiol.* **460** 201–19

[71] Nagarajan S S, Durand D M and Warman E N 1993 Effects of induced electric fields on finite neuronal structures: a simulation study *IEEE Trans. Biomed. Eng.* **40** 1175–88

[72] Amassian V E, Eberle L, Maccabee P J and Cracco R Q 1992 Modelling magnetic coil excitation of human cerebral cortex with a peripheral nerve immersed in a brain-shaped volume conductor: the significance of fibre bending in excitation *Electroencephalogr. Clin. Neurohysiol.* **85** 291–301

[73] Plonsey R and Altman K W 1988 Electrical stimulation of excitable cells—a model approach *Proc. IEEE* **76** 1122–29

[74] Roth B J 1994 Mechanisms for electrical stimulation of excitable tissue *Crit. Rev. Biomed. Eng.* **22** 253–305

[75] Chan C Y and Nicholson C 1986 Modulation by applied electric fields of purkinje and stellate cell activity in the isolated turtle-cerebellum *J. Physiol.* **371** 89–114

[76] Chan C Y, Hounsgaard J and Nicholson C 1988 Effects of electric fields on transmembrane potential and excitability of turtle cerebellar purkinje cells in vitro *J. Physiol.* **402** 751–71

[77] Hause L 1975 A mathematical model for transmembrane potentials secondary to extracellular fields *Electroanesthesia: Biomedical and Biophysical studies* ed A Sances Jr and S J Larson (New York: Academic) pp 176–200

[78] Ghai R S, Bikson M and Durand D M 2000 Effects of applied electric fields on low-calcium epileptiform activity in the CA1 region of rat hippocampal slices *J. Neurophysiol.* **84** 274–80

[79] Gluckman B J, Neel E J, Netoff T I, Ditto W L, Spano M L and Schiff S J 1996 Electric field suppression of epileptiform activity in hippocampal slices *J. Neurophysiol.* **76** 4202–5

[80] Miranda P C, Hallet M and Basser P J 2003 The electric field induced in the brain by magnetic stimulation: a 3-D finite element analysis of the effect of tissue heterogeneity and anisotropy *IEEE Trans. Biomed. Eng.* **50** 1074–85

[81] Amassian V E, Maccabee P J, Cracco R Q, Cracco J B, Somasundaram M, Rothwell J C, Eberle L, Henry K and Rudell A P 1994 The polarity of the induced electric field influences magnetic coil inhibition of human visual cortex: implications for the site of excitation *Electroencephalogr. Clin. Neurophysiol.* **93** 21–6

[82] Krings T, Buchbinder B R, Butler W E, Chiappa K H, Jiang H J, Cosgrove G R and Rosen B R 1997 Functional magnetic resonance imaging and transcranial magnetic stimulation: complementary approaches in the evaluation of cortical motor function *Neurology* **48** 1406–16

[83] Boroojerdi B, Foltys H, Krings T, Spetzger U, Thron A and Topper R 1999 Localization of the motor hand area using transcranial magnetic stimulation and functional magnetic resonance imaging *Clin. Neurophysiol.* **110** 699–704

[84] Wassermann E M, Wang B, Zeffiro T A, Sadato N, Pascual-Leone A, Toro C and Hallet M 1996 Locating the motor cortex on the MRI with transcranial magnetic stimulation and PET *Neuroimage* **3** 1–9

[85] Komssi S, Savolainen P, Heiskala J and Kahkonen S 2007 Excitation threshold of the motor cortex estimated with transcranial magnetic stimulation electroencephalography *Neuroreport* **18** 13–6

[86] Rushton W A H 1927 The effect upon the threshold for nervous excitation of the length of the nerve exposed, and the angle between current and nerve *J. Physiol.* **63** 357–77

[87] Kowalski T, Silny J and Buchner H 2002 Current density threshold for the stimulation of neurons in the motor cortex area *Bioelectromagnetics* **23** 421–8

[88] Francis J T, Gluckman B J and Schiff S J 2003 Sensitivity of neurons to weak electric fields *J. Neurosci.* **23** 7255–61

[89] Durand D M and Bikson M 2001 Suppression and control of epileptiform activity by electrical stimulation: a review *Proc. IEEE* **89** 1065–82

[90] Bikson M, Lian J, Hahn P J, Stacey W C, Sciortino C and Durand D M 2001 Suppression of epileptiform activity by high frequency sinusoidal fields in rat hippocampal slices *J. Physiol.* **531** 181–91

[91] MacDonald D B 2002 Safety of intraoperative transcranial electrical stimulation motor evoked potential monitoring *J. Clin. Neurophysiol.* **19** 416–29

[92] Poreisz C, Boros K, Antal A and Paulus W 2007 Safety aspects of transcranial direct current stimulation concerning healthy subjects and patients *Brain Res. Bull.* **72** 208–14

[93] Merrill D R, Bikson M and Jefferys J G 2005 Electrical stimulation of excitable tissue: design of efficacious and safe protocols *J. Neurosci. Methods* **141** 171–98

[94] Durand D M 2007 Neural engineering – a new discipline for analyzing and interacting with the nervous system *Methods Inf. Med.* **46** 142–6

[95] Oda H and Fujitani Y 1990 Concentric electrodes for producing acupuncture-like anesthetic effects *Tohuku J. Exp. Med.* **160** 169–75

[96] Besio W G, Koka K, Aakula R and Dai W 2006 Tri-polar concentric ring electrode development for laplacian electroencephalography *IEEE Trans. Biomed. Eng.* **53** 926–33

[97] Farina D and Cescon C 2001 Concentric-ring electrode systems for noninvasive detection of single motor unit activity *IEEE Trans. Biomed. Eng.* **48** 1326–34

[98] Besio W, Aakula R, Koka K and Dai W 2006 Development of a tri-polar concentric ring electrode for acquiring accurate laplacian body surface potentials *Ann. Biomed. Eng.* **34** 426–35